Universitat Politècnica de Catalunya (UPC)
Universitat Autònoma de Barcelona (UAB)
Universitat de Barcelona (UB)
Institut de Ciències Fotòniques (ICFO)

http://www.photonicsbcn.eu

Master in Photonics

MASTER THESIS WORK

SPATIAL FILTERING AND COLLIMATION OF THE LIGHT BEAMS BY PHOTONIC CRSYTALS

Lina Maigyte

Supervised by Dr. Kestutis Staliunas, (UPC, ICREA)

Presented on date 19th July 2011

Registered at

Escola Tècnica Superior d'Enginyeria de Telecomunicació de Barcelona

Spatial filtering and collimation of the light beams by Photonic crystals

Lina Maigyte
Group of Nonlinear Dynamics, Nonlinear Optics and Lasers, Departament de Física i Enginyeria Nuclear, Universitat Politècnica de Catalunya, Campus de Terrassa, Terrassa 08022, Spain

E-mail: lina.maigyte@upc.edu

Abstract. Photonic crystals are considered as promising materials for controlling and manipulating the flow of light. In this work we give first experimental evidences of spatial filtering of light beams by three-dimensional ultra-low contrast Photonic crystals made in fused silica glass. Sequentially, we experimentally observe well collimated laser beam by a moderate contrast Photonic crystals of woodpile type. We interpret the observations by theoretical and numerical studies.

Keywords: Spatial filtering, collimation, spatial dispersion, photonic crystal, angular band gap.

1. Introduction: general guidelines

Photonic crystals (PhCs) are dielectric materials with periodically in space varying refraction index on a wavelength scale [1, 2]. For a long time, it was beyond the technological limits to fabricate such structures due to its microscopic origin, however as micro and nano fabrication technologies appeared and rapidly improved during the last decades the fabrication of one-dimensional (1D), two-dimensional (2D) and three-dimensional (3D) photonic structures become possible.

So far, PhCs are associated with well-known properties of temporal dispersion, which yields the ability to design and construct PhCs with photonic band gaps (PBG) - ranges of frequency in which light cannot propagate in the structure [3]. More recently it has been discovered that spatial dispersion (the equivalent of diffraction) can be modified by PhCs as well, which leads to appearance of the angular band gaps of propagating light [4]. There are many other interesting peculiarities in PhCs like vanishing of diffraction or self-collimation of propagating light [5-8]. It is also possible to obtain negative-refraction or super-refraction of light in PhCs [9]. So far, most of propagation effects have been studied in 2D PhCs as they are easier to fabricate than the 3D Photonic crystals [10]. In the Master Thesis we consider and discuss two novel effects we discovered and studied in the group of Nonlinear Dynamics, Nonlinear Optics and Lasers during the period of Master Thesis project: i) spatial filtering with 3D PhCs; ii) collimation of the beam behind the woodpile structured 3D PhCs.

To give a short insight into the work, we briefly present steps which brought us to the results presented in the Master Thesis. Initially, the main goal of the work was to demonstrate spatial filtering by ultra-low contrast PhCs. The goal was successfully achieved and results were published [11]. In continuation, the next step was to achieve more efficient spatial filtering with

the crystals of the higher refraction index. For this reason different kind of PhCs were manufactured. The results were not exactly as expected: instead of obtaining efficient spatial filtering we have observed another interesting effect - collimation of the beams behind the PhCs. The article on latter result has been submitted [12]. We see now that the contrast for the second type of crystals was too high and we should look for intermediate contrast samples to achieve more efficient spatial filtering which will be a natural continuation of research presented in the Master Thesis.

2. Spatial filtering

2.1. Introduction

Many applications in optics require high spatial beam quality, therefore, spatial filtering is broadly used to improve spatial quality of light beams [13]. The traditional technique of spatial filtering uses a confocal system of lenses and a diaphragm of the appropriate diameter [14]. In the Master thesis an alternative method for spatial filtering is explored, i.e., analysed theoretically and demonstrated experimentally. The method is the spatial filtering by PhCs.

PhCs can be utilized to modify spatial dispersion of light beams, by managing the spatial propagation properties of monochromatic light. Conventionally, spatial propagation phenomena is interpreted in terms of the spatial dispersion diagrams, given by the iso-frequency lines of the Bloch modes in $\vec{k}$ - space, i.e., $\omega(\vec{k}) = const.$, which are the spatial dispersion (or diffraction) curves $k_{\parallel}(k_{\perp})$. In isotropic materials the iso-frequency lines are concentric circles, whereas in PhCs the circles are distorted as a result of the periodic modulation of refraction index. The distortion leads to nontrivial spatial propagation effects mentioned in the introduction, in particular to spatial (or angular) filtering [11].

There can be distinguished two types of mechanisms for spatial filtering in PhCs. In the first case: spatial components of the light beam are **reflected backwards** due to distortion of dispersion curves and as a consequence angular band gaps - angles at which the beam cannot propagate - emerge. In another case: the spatial components of the light beam are **deflected** into the first diffraction maxima. Formally, there is no physical band gap in the second case, because spatial components of the light beam travel in forward direction, however spatial filtering of the beam is performed as the components of the light beam are deflected (diffracted) at large angles (angles of the first diffraction maxima of the structure).

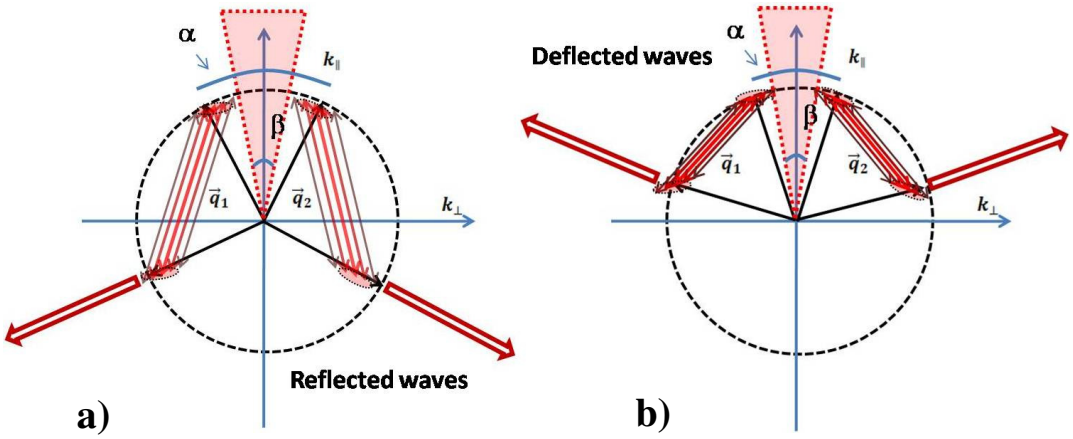

Figure 1. Spatial filtering in reciprocal space $(k_{\perp}, k_{\parallel})$: a) in case of back-reflection and b) in case of forward-deflection.

Both cases are schematically shown in figure 1. The total angular spectrum of incident beams is denoted as α in the figure, the remaining part of spatial spectrum after filtering is denoted by β.

Spatial filtering and collimation of the light beams by the PhCs

The dashed circles in figure 1 correspond to dispersion curves of the homogeneous medium with $|k| = \frac{\omega}{c}$, the radius of the circles is proportional to the frequency. The red arrows inside the circles indicate q vectors of the lattice of the PhC. When the q vector fits into the edges of the dispersion curve (as shown in the figure), modes lying on the dispersion curve get into the resonant condition, they are coupled, and some particular k components of propagating wave which satisfy the resonance condition (ellipses indicated by red) are reflected backwards (Fig. 1 (a)) and others deflected (Fig. 1 (b)) to the first diffraction maxima (cherry coloured arrows indicated in the picture). The basic parameters of the PhC, which determine the range of the wave components to be filtered out and the type of filtering mechanism, are basically longitudinal and transverse periods of the structure. The spatial filtering is possible for the transverse component of the modulation wavevector $q_\perp \leq k$ (equivalently $d_\perp \geq \lambda$). The longitudinal period of the modulation determines the type of filtering mechanism. For the case of reflection (Fig. 1 (a)) the longitudinal wavevector of index modulation must fulfil $2k > q_\parallel > k$, equivalently longitudinal period of index modulation must fulfil $\frac{\lambda}{2} < d_\parallel < \lambda$. For the case of forward deflection (Fig. 1 (b)) longitudinal modulation must fulfil $q_\parallel < k$, equivalently $d_\parallel > \lambda$. The PhCs we were utilizing for spatial filtering were configured for the latter case.

2.2. Samples

Ultra-low refraction index contrast PhCs which were utilized for spatial filtering were fabricated in fused silica glass bulk by selectively applying tightly focused femtosecond laser pulses and this way modifying the refraction index of the material (Fig. 2 (a)) [15-17]. The magnitude of the contrast of refraction index depends on material and exposition conditions and is generally considered to be of the order of 10^{-3} [15-17]. For fabricating the photonic samples the micromachining system with radiation of $\lambda = 1030\,nm$, pulses duration of $\tau = 300$ fs, pulse energy of $E_{imp} = 1\,\mu J$ and repetition rate of $f = 200$ kHz was used. Due to configuration of the system the changed refraction index regions in the PhCs resulted in spots of ellipsoid shape of width of $w_\perp \approx 1\,\mu m$ and of length of $w_\parallel \approx 3\,\mu m$.

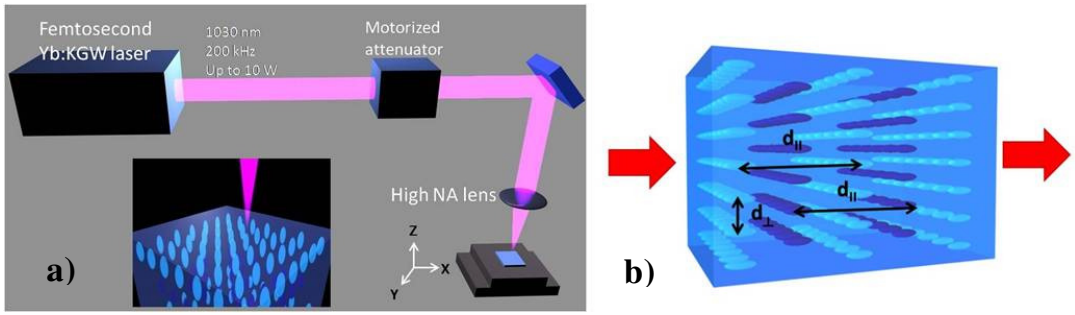

Figure 2. (a) PhC fabrication scheme, (b) the geometry of fabricated PhC where transverse period is $d_\perp = 1.5$ μm and longitudinal period is $d_\parallel = 10.6$ μm.

Figure 2 (b) shows the geometry of the PhC, which consists of odd and even layers marked by differently coloured ellipsoids. The layers are half-period laterally shifted one with respect to the other in the transverse plane. The total number of the longitudinal modulation periods is 25 and each transverse layer contains 500×500 square structure of ellipsoids.

2.3. Experimental results

For illumination of the samples we used two kinds of lasers: 1) CW He-Ne laser of $\lambda = 633\,nm$ with power up to 2mW; 2) CW Nd:YAG laser of $\lambda = 532\,nm$ with power up to 1mW. More recently also a tunable system (wavelength from $0.5\,\mu m$ to $1.3\,\mu m$) with an Optical parametric oscillator (OPO) was used in order to explore the filtering in large frequency range. We focused the beam to fit the PhC well inside the focus. The angular distribution of intensity of transmitted beams was observed (in the far field) on a screen and was also recorded

by a CCD camera, as schematically represented in figure 3 (a). In figure 3 (b) the image of field distribution on a screen is shown where we observed first diffraction maxima at the angles of 21^0. Furthermore, in the central part of the angular field distribution in figure 3 (b) we detect four dark crossing lines which evidence filtered out angular components of the distribution. Figure 3 (c) gives zoom of the central distribution part taken with the CCD camera.

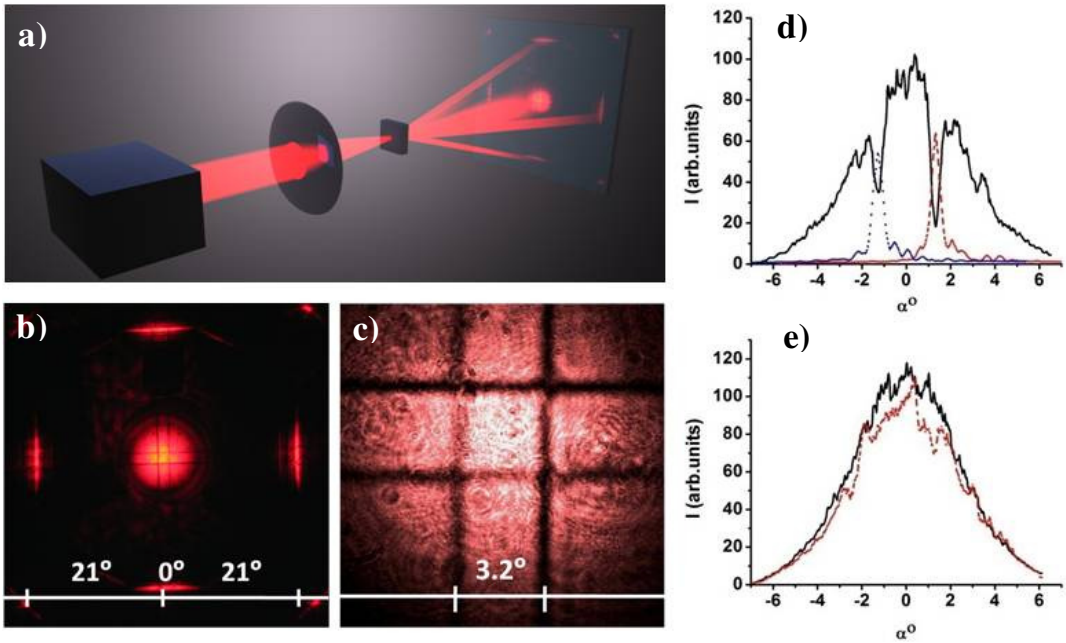

Figure 3. (a) Experimental scheme, (b) image on the screen, (c) CCD camera image of central part of the beam with the filtered out angular field components, (d) intensity distribution of the field from central maximum (solid line) and from the first diffraction maxima (coloured lines), (e) intensity distribution without PhC (solid line) compared with restored intensity distribution (first diffraction maxima are summed with the central part of the beam).

The results we have obtained are highly reproducible (we used several PhC samples manufactured under slightly different conditions) and, as expected, they reveal the signatures of the spatial filtering effect. The crossing dark lines configuration, which can be seen in figure 3 (c), shows the filtered out angular components of the spatial spectra that correspond well with the first diffraction maxima (Fig 3 (b)). Results are in good correspondence with theoretical predictions in the next section.

Figures 3 (d, e) reveal a summary of quantitative analysis of the spatial filtering effect. In figure 3 (d) we find intensity distribution behind the PhC in the far field domain. The result was obtained by horizontal cut, crossing the central part of the beam. The solid black line in the figure stands for the field of the central maximum. The dashed coloured lines correspond to the first diffraction maxima, which were shifted and adjusted to the filtered out angular components (the intensity dips). Figure 3 (d) evidences that the angular intensity distribution of the deflected part of radiation coincides well with the angular distribution of void (dark) parts in the central components. We evaluated from the distributions of the field that approximately 5% of the radiation energy was selectively removed from the central part and deflected into the four first order diffraction maxima, i.e., filtered out.

Figure 3 (e) compares the distribution of the spectra without PhC (black line) with the reconstructed transmitted intensity distribution behind PhC, which we obtained by summing the central part and shifted first diffraction maxima parts of the distribution (red dashed line).

Spatial filtering and collimation of the light beams by the PhCs

2.4.Theory

We use the paraxial approximation for the light propagation in a spatially modulated refraction index material:

$$\left(2ik_0\frac{\partial}{\partial z}+\nabla_\perp^2+2\Delta n(x,y,z)k_0^2\right)A(x,y,z)=0 \quad (1)$$

Here $A(x,y,z)$ stands for the slowly varying complex envelope of the EM field in 3D space propagating along z-direction with the carrier wave-number $k_0 = n\frac{\omega_0}{c}$, where n stands for average refraction index of the material, $\nabla_\perp^2 = \frac{\partial^2}{\partial x^2}+\frac{\partial^2}{\partial y^2}$ means the Laplace operator in the transverse space to the propagation direction.

Harmonic function is used for approximation of the fabricated refraction index profile: $\Delta n(x,y,z) = \frac{\Delta n_0(\cos(q_x x)+\cos(q_y y))\cos(q_z z)}{4}$, where the Δn_0 is the amplitude of the variation of refraction index. We expand the field into harmonic components:

$$A(r_\perp,z) = \int e^{ik_\perp r_\perp}\left(A_0(k_\perp,z)+\sum_{m_x,m_y}A_{m_x,m_y}(k_\perp,z)e^{im_x q_x x+im_y q_y y-iq_z z}\right)dk_\perp \quad (2)$$

The smoothness of the index profile allows as to take into account only the most relevant first order diffraction components $A_{m_x,m_y}(k_\perp,z)$ $\left[(m_x,m_y)=(0,-1),(0,+1),(-1,0),(+1,0)\right]$ and the zero component $A_0(k_\perp,z)$. Integration is performed on the first Brillouin zone, and the sum over the Brillouin zones. The integral (2) is essentially a "folded" inverse Fourier transform. $r_\perp=(x,y)$ refers to the space perpendicular to the propagation direction while $k_\perp=(k_x,k_y)$ indicates the transverse components of the propagation wavevector. Inserting expansion (2) into (1) results in:

$$\frac{d}{dz}A_0 = -\frac{ik_\perp^2}{2k_0}A_0+\frac{i\Delta n_0 k_0}{16}\sum_{m_x,m_y}A_{m_x,m_y} \quad (3.a)$$

$$\frac{d}{dz}A_{m_x,m_y} = \left(-\frac{i(k_x+m_x q_x)^2+i(k_y+m_y q_y)^2}{2k_0}+iq_z\right)A_{m_x,m_y}+\frac{i\Delta n_0 k_0}{16}A_0 \quad (3.b)$$

(3.b) describes a coherent transport of the radiation from the central component $k_\perp=(k_x,k_y)$ to the first diffraction maxima $(k_x+m_x q_x, k_y+m_y q_y)$, and (3.a) brings to depletion of the zero component due to that transport.

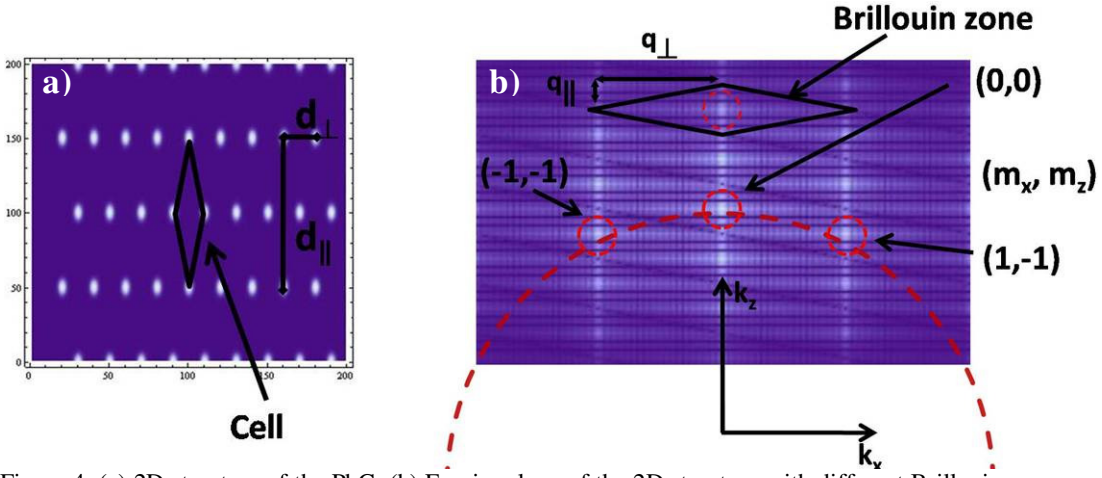

Figure 4. (a) 2D structure of the PhC; (b) Fourier plane of the 2D structure with different Brillouin zones in reciprocal space.

Figure 4 illustrates the situation by showing the distribution of refraction index change in the structure (Fig. 4 (a)). Figure 4 (b) shows Fourier plane with different Brillouin zones. The most efficient scattering and depletion are at the angles $k_\perp$ corresponding to the resonant interaction

between zero component (3.a) and diffracted components (3.b). The resonant condition looks as follows:

$$(k_x + m_x q_x)^2 + (k_y + m_y q_y)^2 - 2q_z k_0 = k_x^2 + k_y^2 \quad (4)$$

and it comes from equation (3). This condition results in four crossing lines in $k_\perp$ space with each line corresponding to a particular set of (m_x, m_y). Physically speaking the radiation from each of the resonance lines is efficiently transported to their "own" diffraction components. The resonant lines refer to the dark lines which were observed in experiment (Fig. 3). The pattern of the lines can be tuned by varying the parameters of the photonic structure.

With the resonant condition (4) it is possible to calculate the angles of the dark lines with respect to the optical axis. For example the resonance line $(m_z, m_y) = (+1,0)$ appears at the position $\frac{k_z}{k_0} = \frac{q_z}{q_x} - \frac{q_z}{(2k_0)}$ in the angular space. The PhCs with the resonance angle of 1.6^0 (Fig. 5 (a)) for the wavelength $\lambda = 633nm$ were designed by using the latter expression.

The formation of the pattern in angular space (Fig. 5) was obtained by numerical integration of (3) and it corresponds well to the scenario observed. In fact, the modulation amplitude of index is not known precisely, therefore we determined it in reverse way: by comparison between experimental figure 3 and numerical calculations shown in figure 5.

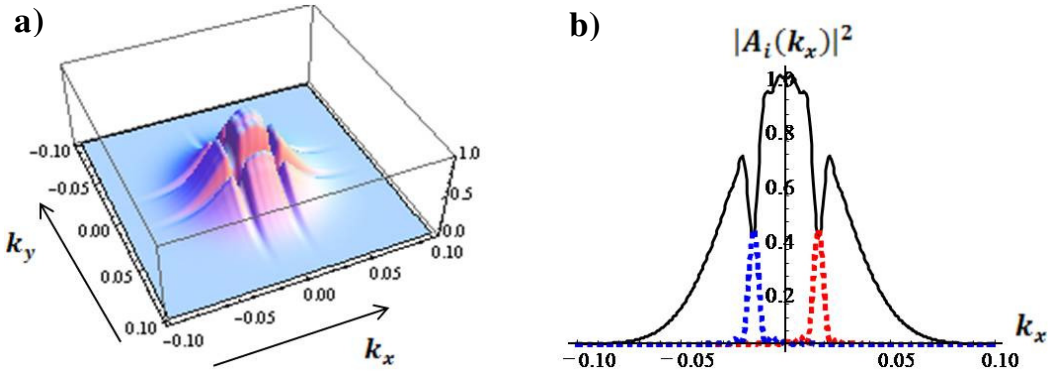

Figure 5. (a) 2D transmission profile; (b) intensity distribution on a horizontal cut.

2.4.1.Discussion

In this way we proved experimentally the effect of spatial filtering of light beams with photonic crystals [11]. However, the result is still far from technological relevance as only approximately 5% of the radiation energy was filtered out. Our objective is to make filtering effect more efficient by filtering out larger angular ranges. In order to optimize the effect we made a series of numerical simulations with different parameters (Mathematica software) (Fig. 6).

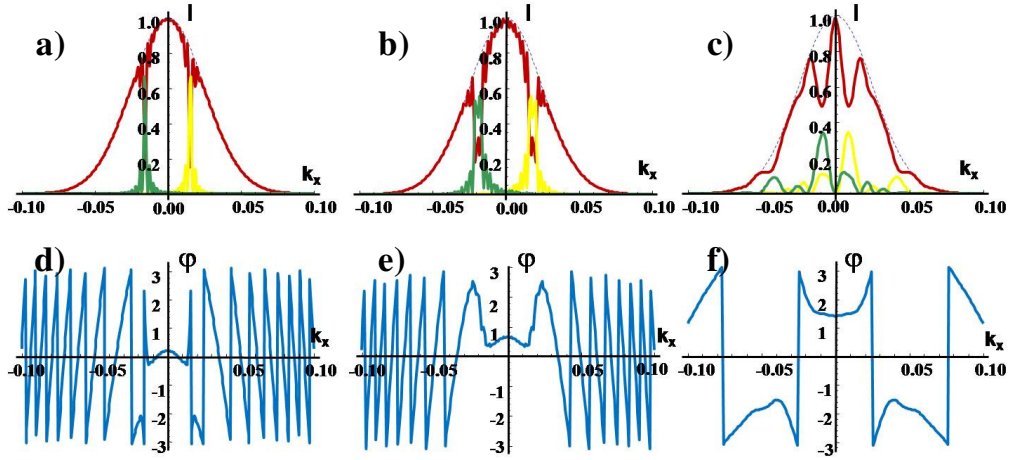

Figure 6. Series of numerical simulations of beam propagation in PhCs, the intensity distributions of central and first diffraction components (upper row) and the phase shift (bottom row).

Spatial filtering and collimation of the light beams by the PhCs

Generally, with the increase of refraction index contrast we obtain broader angles of filtered out regions (Fig. 6 (c)). Therefore, to perform the experiment other kind of PhC samples of woodpile type with moderate refraction index contrast were manufactured (detailed description to be found in the following section). However, speaking in advance, instead of expected broader filtering angle we obtained another peculiar result – collimation of light beams behind the PhC while spatial filtering was negligible. To understand the phenomena we calculated the dispersion curves (Fig. 6 (d, e, f)) corresponding to the intensity distributions above. We observe that the phase shift in cases (d) and (e) have negative curvatures whereas the figure (f) shows positive curvature of dispersion curve. The positive curvature is responsible for negative diffraction of the beams in PhC samples of moderate index contrast, which therefore is responsible for the collimation of the beam behind the PhCs.

The negative diffraction inside the PhC is a key parameter which governs the collimation of beams behind the PhC as mentioned above. Negative diffraction inside the PhC compensates the diffractive broadening of the beam propagating from the focal point, until the front face of the PhC. Therefore the beam wave-fronts are flat on the back-face of the PhC, and the beam continues propagating well collimated. Negative diffraction depends on the parameters of the PhC. Thus, the optimum collimation occurs for a particular distance between the PhC and the focal plane and is determined by the PhC parameters (spatial periods and modulation) (Fig. 7).
We made series of numerical calculations by integrating 2D version of paraxial propagation equation (1). In figure 7 formation of well collimated beams in 2D case is observed.

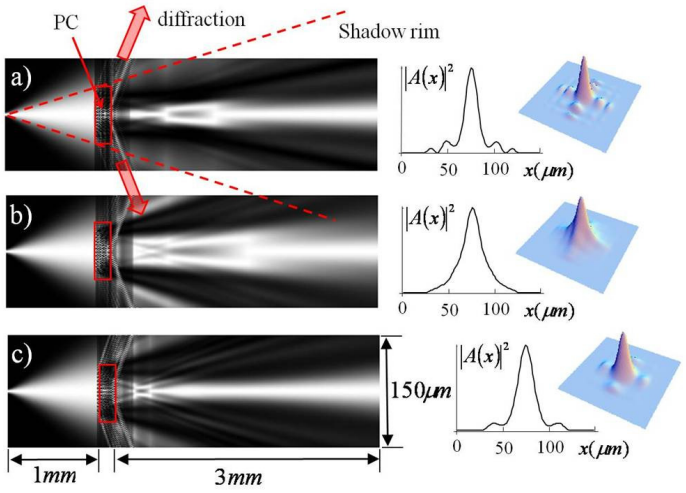

Fig 7. Numerical integration of the paraxial model in 2D of beam propagation inside and behind the PhC with slightly different parameters in (a), (b), (c). 1D figures correspond to the far field domain.

3. Collimation of the beams behind the PhC

3.1. Photonic Crystal samples

The 3D woodpile structured PhC samples were fabricated by femtosecond laser direct writing in photopolymer. The method is described in [18-23]. The photopolymer used was a hybrid organic-inorganic Zr containing SZ080, ensuring high resolution and low geometrical distortions [22]. The woodpile structures of PhCs are composed of parallel photoresist rods arranged into stacked layers. Rods in every other layer are rotated by a 90^0 angle and displaced laterally by a half of transverse lattice period (relative to the previous layer). The structure is illustrated in figure 8 (a). The micrograph by electronic microscope is given in figure 8 (b). Figure 8 (c) and figure 8 (d) are the top and side images of the PhC sample, respectively.
The refractive index contrast of the sample is of the order of 1, so it can be called by moderate contrast sample. The transverse period of the sample is $d_\perp = 1\ \mu m$ and the longitudinal one

$d_{\parallel} = 7{,}8\,\mu m$. The PhC contains 12 periods and consists of 48 layers of rods. Transverse dimensions of the fabricated PhC are 90 µm while the height is 93.6 µm.

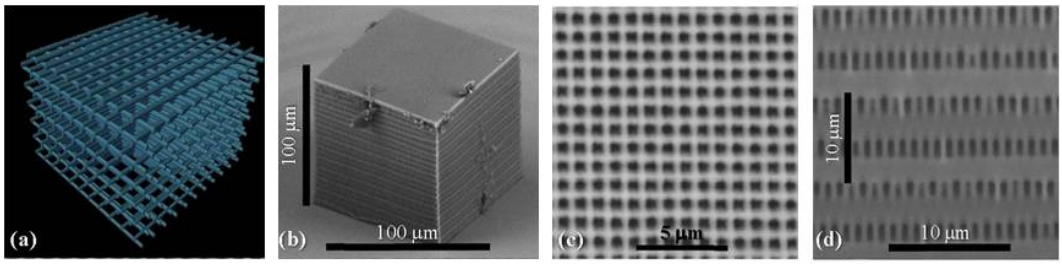

Figure 8. The woodpile PhC sample. (a) illustration of architecture; (b) micrograph by the electronic microscope; (c) top view; (d) side view.

3.2. Experimental results

The experimental setup used for investigation of beam collimation is similar to that used for ultra low contrast crystals (Fig. 3) shown in figure 9 (a).

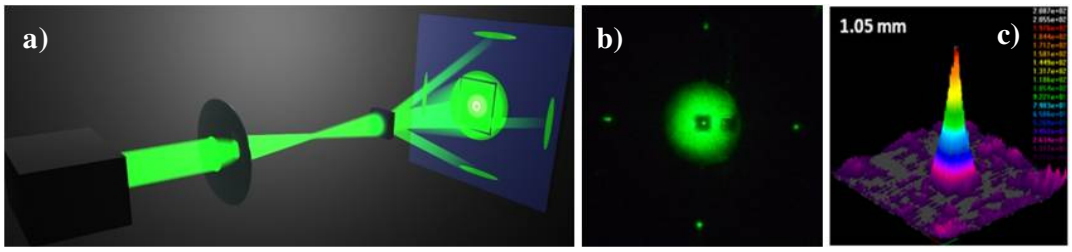

Figure 9. (a) Experimental scheme; (b) Snapshot of far field distribution on a large spatial scale; (c) on small spatial scale.

We used continuous wave Nd:YAG laser with a wavelength of $\lambda = 532\,nm$. The beam was focused by a x10 microscope objective lens to the waist size of $w_0 = 2\,\mu m$ at the focal plane. Woodpile PhC was centered on the optical axis of the beam just behind the focal plane, therefore it was illuminated by a diverging laser beam. The PhC scatters the light, consequently a shadow of the PhC contours is visible (Fig. 9 (b)). Moreover, four first-order diffracted components of the incident beam are observed at angles of 34^0. In addition to this, at the middle of the shadow relatively round spot is detected. The spot corresponds to the collimation effect of the light beam and is the key result of the experiment. We found that the intensity and the shape of the spot are dependent on the distance between the PhC and the focal plane (Fig. 10).

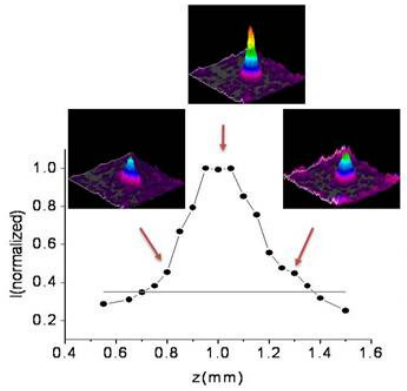

Figure 10. Dependence of the top intensity of the collimated beam on the distance between the focal plane and the PhC.

However, the distance from the PhC to the observation plane (the screen, or camera) doesn't play sensible role for the shape and intensity of the spot.

There exists an optimum distance between the PhC sample and the focal plane where maximum collimation is achieved (Fig. 10), which for given sample was around 1mm. The top intensity of the spot significantly exceeded the irradiation intensity by approximately 4 times, and the width of the beam was 0.12 relative to the width of the shadow of PhC sample. This means that approximately 2% of the shadowed radiation is transformed to the well-collimated beam.

It is important to mention that when PhC sample was being slightly tilted (within 2^0) the spot was remaining at the middle of the shadow. This observation excludes all possible interpretations of effect by the reflections from the surfaces of the sample as well as by a light guiding along the lateral facets.

It may seem that observed picture is similar to the geometrical lensing by the PhC, however, it cannot be interpreted by the ray optics. First of all, PhC samples have a constant thickness over their transverse size, hence we can exclude geometrical lensing due to spherically varying thickness. Moreover, the width of the collimated beam is very weakly sensitive to the distance between the PhC and the focal plane, which would not be the case in geometrical optics. Furthermore, the collimation distance of the propagating beam behind the PhC is relatively long and nowhere shows a sharp focus.

3.4.Summary

The effect of collimation of the beam behind the woodpile 3D PhC sample was experimentally proved for the first time to the best of our knowledge. We have shown that negative diffraction is the key parameter of the PhC which leads to the effect discussed above. However, the full understanding and optimization of the beam formation effect is still a matter of careful theoretical and numerical study. The results from the section 3 are considered for the publication (submitted) [12].

4. Conclusions

To conclude, we have experimentally demonstrated, for the first time to the best of our knowledge, two novel effects of spatial beam propagation through the PhCs:

1) Spatial filtering of the propagating beam in ultra-low index contrast 3D photonic crystal made in fused silica glass.
2) Collimation of the propagating beam behind the moderate index contrast 3D woodpile structured photonic crystal made in polymer.

The spatial filtering effect shown in the Master Thesis carries demonstrational effect only and our future approach is to achieve more significant spatial filtering effect with broader filtering angles.
The filtering, in ideal case, is to be combined with collimation effect.

Acknowledgments

I am indebted to my advisor, Prof. Kestutis Staliunas for his help and encouragement throughout the course of this work. As well I would like to thank to Crina Cojocaru, Jose Trull, Martynas Peckus and Valdas Sirutkaitis for their help and advices in the laboratory. I would like to thank to Marius Rutkauskas, Mangirdas Malinauskas, Titas Gertus, Vygantas Mizeikis and Saulius Juodkazis for fabrication of Photonic crystal samples. This research was funded by the Universitat Politècnica de Catalunya through grant FPI-UPC.

References

[1] Joannopoulos J D, Johnson S G, Winn J N, Meade R D 2008 *Photonic Crystals: Molding the Flow of Light* (Princeton University Press)
[2] Mizeikis V, Juodkazis S, Marcinkevičius A, Matuso S and Misawa H 2001 Tailoring and characterization of photonic crystals *J. Photochem. Photobiol C.* **2** 35-69
[3] Yablonovitch E 1987 Inhibited spontaneous emission in solid-state physics and electronics *Physic. Rev. Lett.* **58** 2059-2062
[4] Staliunas K and Sánchez-Morcillo V J 2009 Spatial filtering of light by chirped photonic crystals *Phys. Rev. A* **79** 053807
[5] Zengerle R 1987 Light propagation in singly and doubly periodic planar waveguides *J. Mod. Opt.* **34** 1589-1617
[6] Kosaka H, Kawashima T, Tomita A, Notomi M, Tamamura T, Sato T and Kawakami S 1999 Self-collimating phenomena in photonic crystals *Appl. Phys. Lett.* **74** 1212
[7] Dholakia K and Reece P 2006 Optical micromanipulation takes hold *Nanotoday* **1** 18-27
Chigrin D N *et al.* 2003 Self-guiding in two-dimensional photonic crystals *Opt. Exp*. **11** 1203- 12011
[8] Staliunas K and Herrero R 2006 Nondiffractive propagation of light in photonic crystals *Phys. Rev. E* **73** 016601
[9] Lupu A, de Lustrac A, Ourir A, Checoury X, Lourtioz JM, Centeno E, Cassagne D, Albert JP, Pommereau F, Legouezigou L, Drisse O, Legouezigou O, Deroin E, Duan GH 2006 Discontinuous wavelength super-refraction in photonic crystal superprism *Opt. Exp* **14** 2003-2013
[10] Baumberg J J, Perney N M B, Netti M C, Charlton M D C, Zoorob M and Parker G J 2004 Visible-wavelength super-refraction in photonic crystal superprisms *App. Phys. Lett.* **85** 354
[11] Maigyte L, Gertus T, Trull J, Cojocaru C, Sirutkaitis V and Staliunas K 2010 Signatures of light-beam spatial filtering in a three-dimensional photonic crystal *Phys. Rev. A* **82** 043819
[12] Trull J, Maigyte L, Mizeikis V, Malinauskas M, Juodkazis S, Cojocaru C, Rutkauskas M, Peckus M, Sirutkaitis V and Staliunas K 2011(submitted) Formation of collimated beams by woodpile Photonic crystals *Phys. Rev. A*
[13] Siegman A E 1993 Defining, measuring, and optimizing laser beam quality *Proc.SPIE* 1868 2
[14] Hariharan P 1996 *Optical holography* (Cambridge University Press)
[15] Kamata K and Obara M 2004 Control of the refractive index change in fused silica glasses induced by a loosely focused femtosecond laser *Appl. Phys. A* **78** 85
[16] Gattas R R and Mazur E 2008 Femtosecond laser micromachining in transparent materials *Nature photonics* **2** 219
[17] Streltsov A M, Borrelli N F 2002 Study of femtosecond laser-written waveguides *JOSA B* **19** 2496
[18] Serbin J, Ovsianikov A and Chichkov B Fabrication of woodpile structures by two-photon polymerization and of their optical propertiesN 2004 *Opt. Express* **12** 5221
[19] Deubel M, von Freymann G, Wegener M, Pereira S, Busch K, Soukoulis K M 2004 Direct laser writing of three-dimensional Photonic crystal-crystal tamplates for telecommunications *Nature Materials* **3** 444
[20] Mizeikis V, Seet K K, Juodkazis S, and Misawa H 2004 Three-dimensional woodpile Photonic crystal templates for the infrared spectral range *Opt. Lett.* **29** 2061
[21] LaFratta C N, Fourkas J T, Baldacchini T, Farrer R A 2007 Multiphoton Fabrication *ChemInform* **38** 45
[22] Ovsianikov A, Viertl J, Chichkov B, Oubaha M, *et al.* C 2008 Ultra-low Shrinkage Hybrid Photosensitive material for two-photon Polymerization Microfacbrication *ACS Nano* **2** 2257
[23] Malinauskas M, Žukauskas A, Bičkauskaitė G, Gadonas R, Juodkazis S 2010 Mechanisms of three-dimensional structuring of photo-polymers by tightlyfocussed femtosecond laser pulses *Opt. Express* **18** 10209